

Effect of orientation on ion track formation in apatite and zircon

WEIXING LI^{1,*}, PATRICK KLUTH², DANIEL SCHAURIES², MATIAS D. RODRIGUEZ², MAIK LANG¹,
FUXIANG ZHANG¹, MAXIM ZDOROVETS³, CHRISTINA TRAUTMANN⁴ AND RODNEY C. EWING^{1,5,†}

¹Department of Earth & Environmental Sciences, University of Michigan, Ann Arbor, Michigan 48109-1005, U.S.A.

²Department of Electronic Materials Engineering, Research School of Physics and Engineering, The Australian National University, Canberra, ACT 0200, Australia

³Institute of Nuclear Physics, and The L.N. Gumilyov Eurasian National University, Astana, 010008, Kazakhstan

⁴GSI Helmholtz Centre for Heavy Ion Research, 64291 Darmstadt, and Technische Universität Darmstadt, Germany

⁵Departments of Materials Science & Engineering, and Nuclear Engineering & Radiological Sciences, University of Michigan, Ann Arbor, Michigan 48109-2104, U.S.A.

ABSTRACT

Fission track (FT) thermochronology is essentially based on empirical fits to annealing data of FTs revealed by chemical etching, because, until now, unetched, latent FTs could not be examined analytically at the atomic-scale. The major challenge to such an analysis has been the random orientation of FTs and their extremely small diameters. Here we use high-energy ions (2.2 GeV Au or 80 MeV Xe) to simulate FT formation along specific crystallographic orientations. By combining results from transmission electron microscopy (TEM) of single tracks and small-angle X-ray scattering (SAXS) for millions of tracks, a precise picture of track morphology as a function of orientation is obtained. High-resolution analysis reveals that orientation affects the shape of tracks in apatite and zircon through the preferential creation of damage along directions with highest atomic density. However, track radius does not depend on orientation, contradicting previous reports. Independent of track orientation, track radii, as measured at each point along the entire length of 80 MeV Xe ion tracks in apatite, can be understood using the thermal spike model of Szenes. Thus, the well-known track annealing anisotropy of apatite is not due to track radius anisotropy. The combination of ion-irradiations with TEM and SAXS analysis provides a unique opportunity to understand and model track formation and annealing under various geologic conditions.

Keywords: Ion tracks, fission tracks, apatite, zircon, orientation effects, thermal spike, TEM, SAXS

INTRODUCTION

Swift heavy ions (SHIs) create a narrow track of damage in an irradiated solid along the trajectory of the ion. Such SHI irradiations have widespread applications in nanoengineering (Akcoltekin et al. 2007; Mara et al. 2004), and particle damage in electronics (Dodd and Massengill 2003). More interestingly, SHI irradiations can be used to simulate the formation of fission tracks (FTs), damage trails that were caused by spontaneous fission events of uranium impurities in minerals that have been widely used for age dating and thermochronology (Donelick et al. 1999; Gleadow et al. 2002; Jonckheere and Chadderton 2002; Yamada et al. 1995). Generally, tracks in transverse cross section are circular, but in a few cases (Bursill and Braunshausen 1990; Hebert et al. 1998; Paul and Fitzgerald 1992; Vetter et al. 1994), they have a tendency to facet along specific crystallographic directions, with an important indication that orientation may play a role in track formation. However, details of how orientation affects track formation remain elusive, because there are very few systematic studies of the shape and radius of latent,

unetched tracks as a function of orientation at the atomic-scale. According to a highly cited transmission electron microscopy (TEM) study (Paul and Fitzgerald 1992), the mean radius ($\sim 4.5 \pm 3.7$ nm) of latent FTs $\parallel c$ (or the c axis) of the hexagonal apatite [$\text{Ca}_{10}(\text{PO}_4)_6\text{F}_2$] is significantly larger than that ($\sim 2.5 \pm 2.8$ nm) of FTs $\perp c$. The anisotropy of track radii in apatite has gained general acceptance (Carlson 1993; Jaskierowicz et al. 2004; Rabone et al. 2008; Schouwink et al. 2010), and has been used to explain (Carlson 1993; Paul and Fitzgerald 1992) the well-known track annealing anisotropy (Donelick et al. 1999; Gleadow et al. 2002; Green and Durrani 1977), i.e., tracks $\parallel c$ anneal more slowly than tracks $\perp c$, however, a molecular dynamics simulation concluded that track size was insensitive to orientation (Rabone et al. 2008). Because of the random orientation of FTs, TEM imaging of the track radius requires considerable effort to accurately determine the orientation of any individual track that is measured, essentially requiring the alignment of the electron beam parallel to major zone axes of the grain. In this study, we overcome this problem by investigating parallel tracks produced by the irradiations of SHIs (2.2 GeV Au or 80 MeV Xe) along known zone axes of apatite ($P6_3/m$) and zircon (ZrSiO_4 ; $I4_1/amd$), two minerals that have anisotropic structures and figure prominently in FT thermochronology. By combining the results from TEM analysis of single tracks and small-angle

* E-mail: wxli@umich.edu

† Present address: Department of Geological & Environmental Sciences, Stanford University, Stanford, CA 94305, U.S.A.

X-ray scattering (SAXS) for millions of tracks (Afra et al. 2011), a precise picture of track morphology as a function of orientation is obtained. High-resolution TEM analysis reveals how orientation affects track shape and size at the atomic scale. Using the microtome cutting method and the thermal spike model, we compare variations in radius at each point along the entire length of 80 MeV Xe ions in apatite $\parallel c$ and $\perp c$.

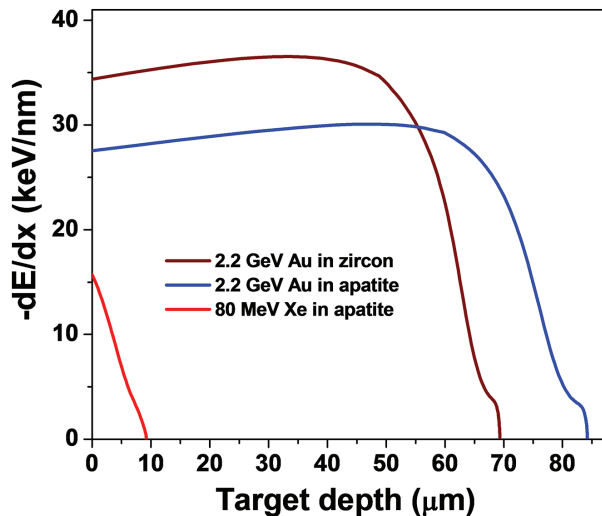


FIGURE 1. The electronic energy loss per unit length, $(-dE/dx)_e = S_e$, as a function of target depth, x , for the irradiations of 2.2 GeV Au ions in zirconon, 2.2 GeV Au ions in apatite, and 80 MeV Xe ions in apatite, respectively. (Color online.)

EXPERIMENTAL METHODS

Two types of SHIs were used in this study. For the 2.2 GeV Au ion irradiation experiments, the ion range is ~ 70 and $85 \mu\text{m}$, as calculated by the SRIM code (Ziegler et al. 2010), for zirconon and apatite, respectively (Fig. 1). The electronic energy loss per unit length, or stopping power, $(-dE/dx)_e = S_e$, as a function of target depth was calculated by SRIM simulation with the function of Calculate Quick Range Table. The densities of apatite and zirconon were set as 3.2 and 4.52 g/cm^3 , respectively. The total number of runs (or ions) was set $10\,000$ to calculate ion distribution and damage along the ion trajectories. The SRIM simulation shows that the angle of each track deviated from the original trajectory for the 2.2 GeV Au ion is negligibly small, especially at the lower target depths ($< 40 \mu\text{m}$). The samples were pre-polished to a thickness $\sim 40 \mu\text{m}$ to ensure that the GeV projectiles completely penetrate the sample thickness, inducing an approximately uniform energy deposition, $-dE/dx$, and producing a nearly constant track radius throughout the entire sample thickness (Li et al. 2013). In contrast, as the 80 MeV Xe ions, which have a typical mass and energy of fission fragments, slow down, $-dE/dx$ decreases (Fig. 1), resulting in a significantly smaller track radius in apatite toward the end of the track (Li et al. 2012). Variations in radius along the entire length (up to $8.1 \mu\text{m}$) of ion tracks along the c -axis of apatite were first obtained by the microtome method (Li et al. 2012). For a fission fragment (e.g., 80 MeV Xe ion), the track range that can be observed by TEM is $\sim 2 \mu\text{m}$ (Li et al. 2012) less than the ion range because the energy at its very end falls below the energy threshold required to produce an observable track. Although the energy of 2.2 GeV Au is significantly larger than that of a typical fission fragment, the difference in $-dE/dx$ is small at the point of impact (for apatite: $\sim 27 \text{ keV/nm}$ for 2.2 GeV Au vs. $\sim 16 \text{ keV/nm}$ for 80 MeV Xe) (Fig. 1). More importantly, this difference in $-dE/dx$ does not result in significant differences in the track morphology (Li et al. 2010).

Tracks ($\parallel c$ or $\perp c$) were produced in bulk samples $\sim 40 \mu\text{m}$ thick by exposing (0001) and $(5\bar{1}40)$ surfaces of Durango fluorapatite, and (001) and (100) surfaces of synthesized single-crystal zirconon, respectively, to 2.2 GeV Au ions in $5 \times 10^{10} \text{ ions/cm}^2$ at normal incidence at the UNILAC accelerator, GSI, Darmstadt, Germany. Without further preparation, bulk samples were investigated after irradiation using transmission SAXS at the Australian Synchrotron in Melbourne, Australia. See Kluth et al. (2008) and Li et al. (2013) for details of the SAXS measurements. TEM studies were completed with a JEOL 3011 electron microscope. The irradiated bulk samples were crushed and suspended on a carbon film supported by Cu grid for

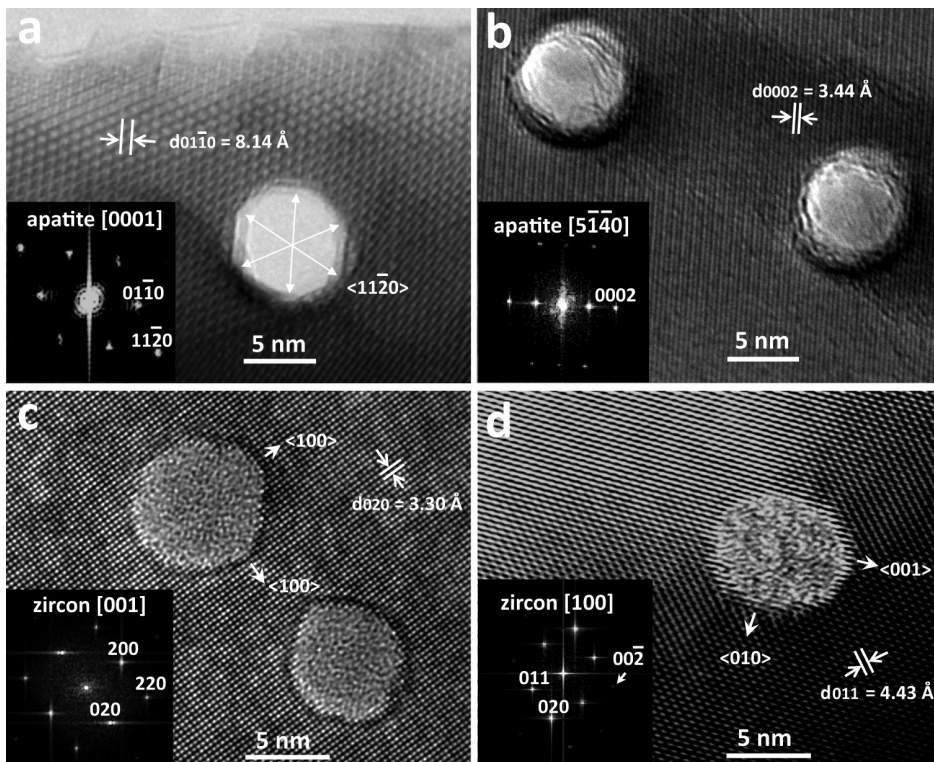


FIGURE 2. Transverse cross-section HRTEM images of tracks induced by exposure to 2.2 GeV Au ions $\parallel c$ or $\perp c$ of apatite and zirconon. The track orientation (or the zone axis of the target material) was determined by indexing the inset of fast Fourier transform image for each figure.

the TEM studies. To simulate FTs, tracks $\parallel c$ or $\perp c$ of apatite were produced by irradiating a single crystal $\sim 200 \mu\text{m}$ thick with 80 MeV Xe ions to a fluence of 5×10^{10} ions/cm² at the Cyclotron DC-60 at the National Nuclear Centre in Kazakhstan. Cross-sectional TEM specimens containing parallel tracks were prepared by cutting the irradiated sample along their ion trajectories ($\parallel c$ or $\perp c$) with a diamond knife in a microtome to show variations in track radius along the entire track. See Li et al. (2012) for details of the microtome method.

RESULTS AND DISCUSSION

2.2 GeV Au ions

High-resolution TEM (HRTEM) analysis of 2.2 GeV Au tracks was obtained in transverse cross section, i.e., tracks are parallel to electron beam, by carefully tilting a crushed specimen to align its zone axis ($\parallel c$ or $\perp c$), which is parallel to the tracks in this case, to the incident electron beam. In apatite, the central core region of the tracks has the same bright contrast as the free space (Figs. 2a, 2b, and 3a), indicating the highly porous nature of tracks, as has been discussed in detail in (Li et al. 2010). This is significantly different from the amorphous core region of tracks in zircon (Figs. 2c, 2d, and 3b). For each track $\parallel c$ of apatite, there is clear hexagonal faceting (Fig. 2a) (Paul and Fitzgerald 1992), as compared with the circular tracks $\perp c$ (here along $[5\bar{1}40]$) (Figs. 2b and 3a). In a fast Fourier transformation (FFT) image, a vector pointing from (0000) to a diffraction spot represents the corresponding crystal direction in the imaging plane. Thus, the preferential faceting directions in Figure 2a can be determined as the six equivalent, close packed $\langle 11\bar{2}0 \rangle$ directions, which are parallel to the six diagonals of a hexagonal projection onto (0001) for etched tracks $\parallel c$ (Jonckheere and VandenHaute 1996; Paul and Fitzgerald 1992). In zircon, tracks along $[001]$ appear to be approximately square in shape (Fig. 2c) with the

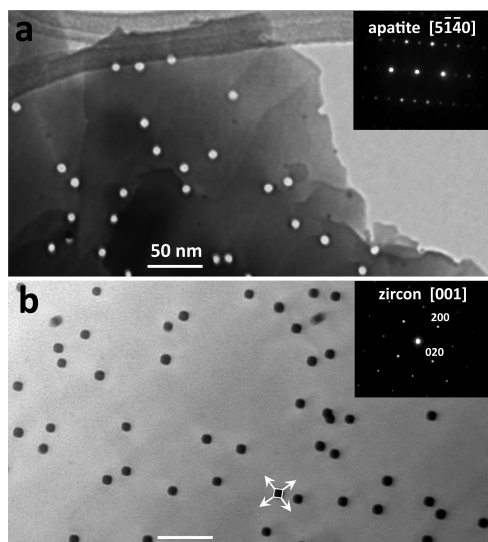


FIGURE 3. Conventional transverse cross-section TEM images (under focus and bright-field) show multiple tracks in (a) apatite and (b) zircon. The areal densities of the 2.2 GeV Au ions induced tracks for both materials are consistent well within the nominal ion density (5×10^{10} ions/cm²). The track orientation (or the zone axis of the target material) was determined by indexing the inset of diffraction pattern for each figure. A track in **b** marked with the white arrows and square as a guide to the eye, is a representative of multiple square tracks with diagonals pointing in the $\langle 100 \rangle$ directions.

diagonals parallel to the four equivalent $\langle 100 \rangle$ directions, as this tendency can be further confirmed in a low-magnification image (Fig. 3b), which shows multiple square tracks with the diagonals pointing in the same directions. Within the (001) plane, the atomic density is highest along the $\langle 100 \rangle$ directions, similar to the case in the close-packed directions. Tracks along $[100]$ of zircon appear to be elliptical with the long axis in the $\langle 001 \rangle$ direction, which have the highest atomic density within the (100) plane (Fig. 2d). The ratio (1.106) of the long axes to the short axes (7.8 vs. 7.1 nm) in Figure 2d corresponds to the reciprocal ratio of the unit-cell constants ($a/c = 1.105$), as well as the corresponding d spacings ($d_{200}/d_{002} = 1.105$). This is similar to the case for GeS, where the long axis of the elliptical tracks are parallel to the close-packed $\langle 001 \rangle$ direction (Vetter et al. 1994). Thus, the atomic-scale resolution reveals that the shape of tracks in apatite and zircon depends on track orientation in the crystal as a result of preferential creation of radiation damage along the directions with highest atomic density.

As the scale bar can be precisely calibrated by the known d spacings (Fig. 2), the mean track radius can be measured reliably: 4.0 ± 0.2 nm for tracks $\parallel c$ vs. 3.9 ± 0.4 nm for tracks $\perp c$ in apatite; 3.8 ± 0.4 nm for tracks $\parallel c$ vs. 3.7 ± 0.4 nm for tracks $\perp c$ in zircon, which is consistent with a previous HRTEM measured radius (~ 4 nm) for 2.9 GeV Pb ion induced tracks $\perp c$ of zircon (Bursill and Braunshausen 1990). The mean radius was determined by averaging the radii of approximately 5 tracks for each orientation ($\parallel c$ or $\perp c$) in apatite and zircon. Within the errors, the HRTEM measured track radii are actually indistinguishable for the different orientations. However, the track shape changes significantly for the different orientations.

In addition to the images of tracks in transverse cross section, the structure and morphology of tracks can be viewed in longitudinal cross section, i.e., tracks are perpendicular to the electron beam by the under focus low-magnification images (Fig. 4). For apatite, the average radius of tracks $\parallel c$ and $\perp c$ is 4.6 ± 0.4 and 4.6 ± 0.5 nm, respectively. For zircon, the average radius is 4.3 ± 0.4 nm $\parallel c$, close to 4.1 ± 0.5 nm for $\perp c$. Ten tracks were measured for each orientation. Thus, the mean values of the track radii are insensitive to orientation, which is consistent with the HRTEM measurements.

As compared with the limited number of tracks in a localized area as observed by TEM, the strong scattering oscillations, as detected by SAXS from a very large number of well aligned, identical tracks in a bulk sample, provide an extremely reliable means for determining the mean track radius. The scattering intensities of tracks and corresponding analytical fits to the hard cylinder model (Afra et al. 2011; Li et al. 2013) are shown in Figure 5. The GeV Au ions induce tracks $\parallel c$ of apatite with a mean radius of 4.81 ± 0.03 nm, which is slightly larger than that (4.72 ± 0.03 nm) of tracks $\perp c$. In zircon, the mean track radius $\parallel c$ is 4.43 ± 0.03 nm, slightly larger than that (4.32 ± 0.03 nm) of tracks $\perp c$. The SAXS measurements are consistent with the TEM measurements in that the mean radii of tracks $\parallel c$ are very close to those of tracks $\perp c$.

80 MeV Xe ions

In addition to the GeV ions, the influence of track orientation on track radius was investigated by TEM comparing the damage at each point along latent tracks created by 80 MeV Xe ions $\parallel c$ or $\perp c$ of apatite (Fig. 6). Using the microtome method (Li et

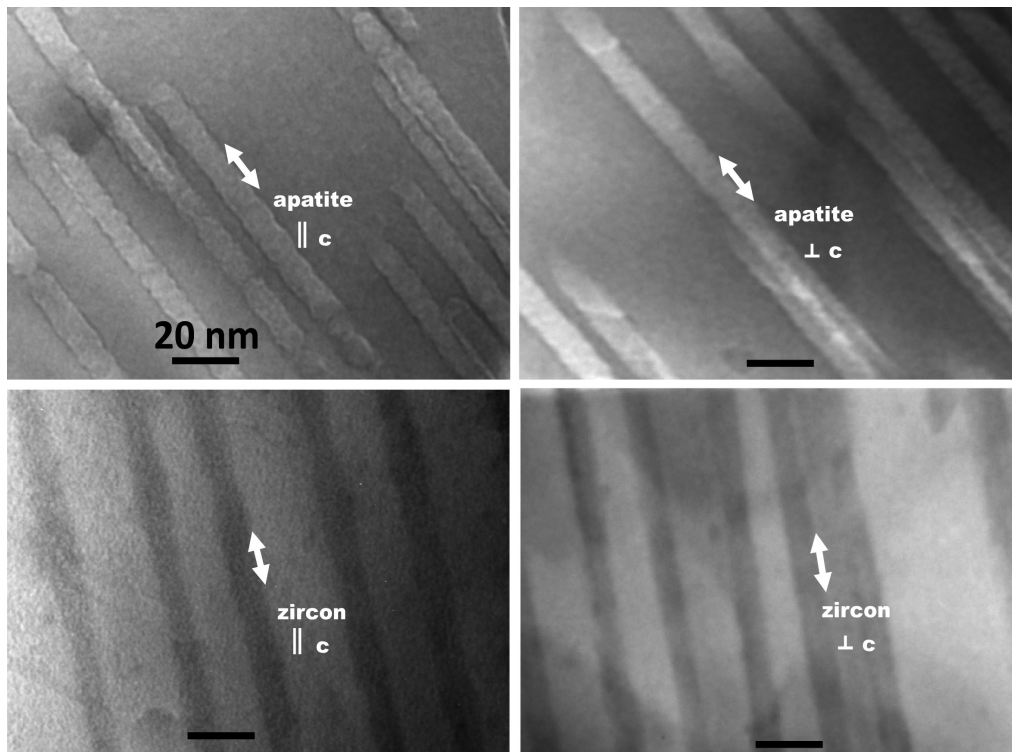


FIGURE 4. Conventional TEM images (under focus and bright-field) show tracks (viewed in longitudinal cross section) induced by exposure to 2.2 GeV Au ions $\parallel c$ or $\perp c$ of apatite or zircon, as marked in each image.

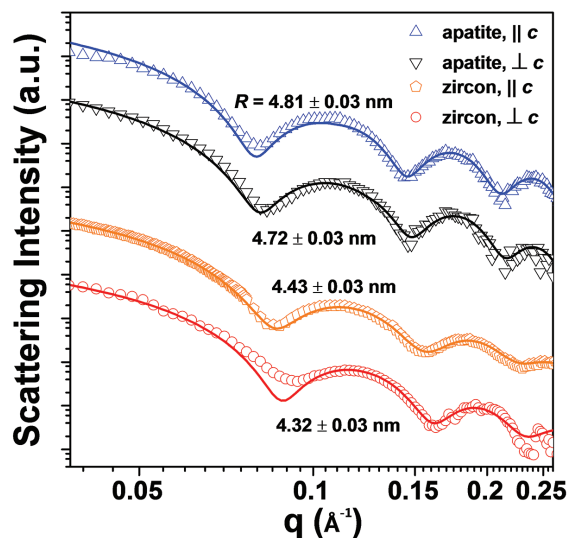


FIGURE 5. SAXS measurements showing scattering intensities of 2.2 GeV Au ion induced tracks $\parallel c$ or $\perp c$ of apatite and zircon as a function of the scattering vector q , and corresponding fits with the hard cylinder model (solid lines). The errors of track radii correspond to the uncertainty of the fitting. (Color online.)

al. 2012), the track profile was obtained by taking a series of images along the ion paths (Figs. 6a–6d). Three examples of under focus TEM images of tracks $\perp c$ measured at different depths ($x = 0, 3,$ and $6.7 \mu\text{m}$) from the ion-irradiated surface are

shown in Figures 6a to 6c. Approximately 10 tracks were measured at each target depth. The changes of track radii along the ion paths $\parallel c$ and $\perp c$ in apatite are plotted in Figure 6e. Within experimental error, the mean radii for tracks $\perp c$ are very close to the radii of tracks $\parallel c$ at almost all the depths. This provides direct evidence that latent ion tracks in apatite do not have different sized radii as a function of orientation, in contrast to the previous observation of significantly larger FTs $\parallel c$ than those $\perp c$ in apatite (Paul and Fitzgerald 1992). This discrepancy is due to the difficulty of determining the precise orientation of any individual track [of the total 293 randomly orientated FTs that were measured (Paul and Fitzgerald 1992)]. For complex materials (e.g., apatite) where different zones may have similar diffraction patterns, the incorrect indexing of the zone axis of a grain is possible. Furthermore, because it is impossible to determine the target depth of a randomly orientated FT by TEM, the decrease in radius along a FT, as clearly shown in Figure 6, could not be considered, resulting in significantly larger errors.

For both track directions, the decrease in track radius per unit depth, $-dR/dx$, is relatively low at shallower depths ($0 \leq x \leq 3.5 \mu\text{m}$). The track radii at shallower depths (Figs. 6a and 6b) can be described by a relation of $R \sim S_e^{1/2}$ (Fig. 6e), as this relation was applied to tracks in $\text{Y}_2\text{Fe}_5\text{O}_{12}$ (Szenes 1995). However, at greater depths ($x \geq 3.5 \mu\text{m}$) (Fig. 6c), R falls below the curve of $R \sim S_e^{1/2}$, as the $-dR/dx$ is obviously higher than that at the shallower depths (Fig. 6e). The $-dE/dx$ as a function of target depth x was simulated by the SRIM code (Ziegler et al. 2010) and R was measured at different depths by TEM (Fig. 6e). Therefore, R as a function of $-dE/dx$ for both directions can be obtained, and

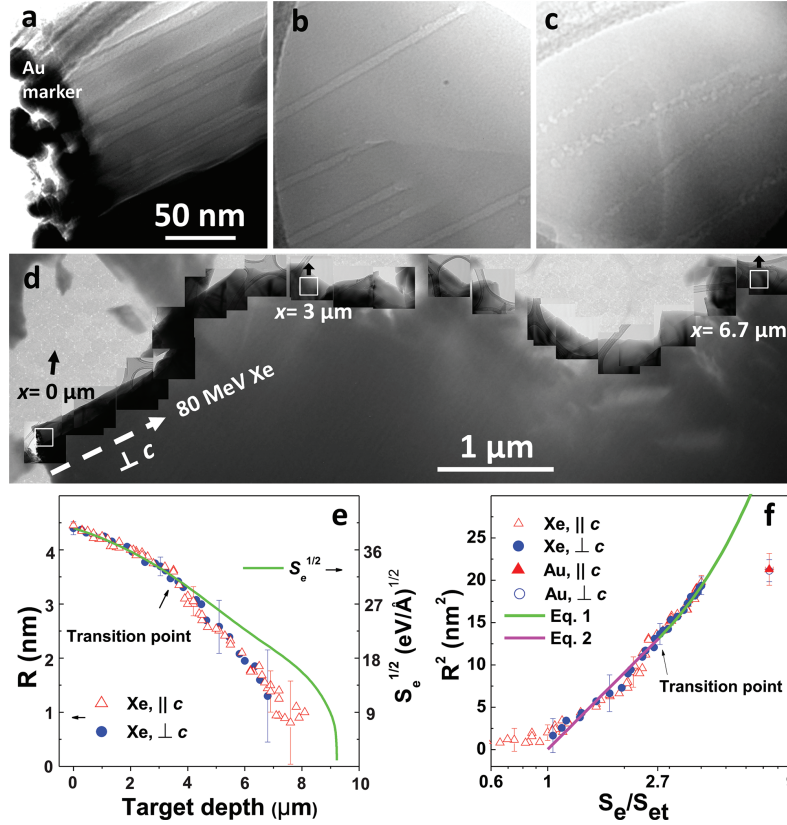


FIGURE 6. A comparison of variations in radius at each point along the tracks induced by the irradiation of 80 MeV Xe ions $\parallel c$ and $\perp c$ of apatite. (a to c) Three examples of conventional TEM images (under focus and bright-field) of tracks $\perp c$, taken at different depths from the ion irradiated surface along the whole length of a microtome section, as marked in a lower magnification image. (d) A thin layer of gold was deposited on the irradiated surface as a surface marker. (e) Mean track radii, R , almost overlap along the tracks of the two directions. $R \sim S_e^{1/2}$ at smaller target depths. (f) Variations in track radius vs. S_e normalized to the threshold value of S_{et} can be understood in terms of the Szenes model. (Color online.)

these values are plotted in Figure 6f. These data were compared with the theoretical prediction from the thermal spike model of Szenes (1995). Depending on the value of S_e , the track radius R (the maximum radius of the melt during the heating-cooling process) can be determined by two different expressions (Szenes 1995). For $S_e \geq 2.7S_{et}$, the melted zone expands and reaches its maximum,

$$R^2 = [a_0^2/2.7](S_e/S_{et}) \quad (1)$$

where S_{et} is the threshold energy for the production of continuous tracks. a_0 relates to thermal diffusivities, but it can be determined by fitting. This expression is consistent with our analysis shown in Figure 6e that $R \sim S_e^{1/2}$ for tracks at shallower depths. For $2.7 \geq S_e/S_{et} \geq 1$, the melted zone shrinks with time, and it has the maximum radius at $t = 0$ when the cooling spike begins,

$$R^2 = a_0^2 \ln(S_e/S_{et}). \quad (2)$$

This regime ($2.7 \geq S_e/S_{et} \geq 1$) corresponds to tracks at greater depths where the values of S_e are smaller (Fig. 6c). There is a smooth transition from the logarithmic to linear regimes, as both Equations 1 and 2 provide the same R^2 at $S_e = 2.7S_{et}$. In this study,

the transition point is at $x \sim 3.5 \mu\text{m}$ in Figure 6e. Thus, the corresponding two parameters for the fits ($R = a_0 = 3.6 \text{ nm}$, $S_e = 2.7S_{et} = 1065 \text{ eV/\AA}$) can be directly determined from the transition point in Figure 6e. As shown in Figure 6f, all experimental data for 80 MeV Xe ions follow a single curve as a good approximation in both the logarithmic and linear regimes. The data for the 2.2 GeV Au induced tracks (measured from Figs. 4a–4b) are below the curve (Fig. 6f). This is due to the velocity effect (Meftah et al. 1993), which describes the decrease of track radius with the ion speed at certain high energy regimes.

IMPLICATIONS

Hexagonal apatite has an open anion channel $\parallel c$ (Calderin et al. 2003), with possible implications for anisotropy in the annealing of fission tracks. The exact details of how structural anisotropy affects anisotropic annealing behavior remain unclear, although there is certainly a connection between the two types of anisotropy (Gleadow et al. 2002; Green and Durrani 1977). The slower annealing rate of tracks $\parallel c$ is attributed to the larger tracks $\parallel c$ (Paul and Fitzgerald 1992). Besides the weaker intermolecular bonds along the c -axis (Paul and Fitzgerald 1992), smaller dielectric constants $\parallel c$ has been used to explain the larger tracks along this direction (Rabone et al. 2008). In this study, except

for the orientation-related difference in track shape as discussed above, the detailed TEM and SAXS experimental evidence on parallel tracks with well-defined orientations in the structure clearly demonstrates that the track radii have no apparent dependence on track direction in apatite, which is in agreement with a previous molecular dynamics simulation (Rabone et al. 2008). Based on the direct observation of in situ thermal annealing of unetched FTs in apatite (Li et al. 2011), the annealing anisotropy as observed in chemically etched tracks can be attributed to the preferential motion of FT segments $\parallel c$ during annealing. Similarly, no obvious track radius anisotropy was detected in zircon by the TEM and SAXS measurements, although zircon is structurally anisotropic with a chain of alternating edge-sharing SiO_4 tetrahedra and ZrO_8 triangular dodecahedra extending $\parallel c$ (Robinson et al. 1971).

Currently, FT thermochemistry is based almost entirely on empirical fits to annealing data of FTs revealed by chemical etching. One of the main obstacles to quantitative modeling of FT behavior has been the need to investigate the morphology of latent tracks as a function of temperature and time. For a single track created by a fission fragment pair, the radius is largest near the midpoint of track where the fission event occurs, and decreases toward each end as the S_e decreases, as shown in Figure 1. At elevated temperatures, the etchable track length is gradually reduced from each end of a FT toward the midpoint because the track ends have much smaller radii, and anneal much more rapidly, which was observed by in situ TEM (Li et al. 2012). As a result, only the sections with smaller S_e (as well as R) near each end of the FT make a major contribution for the length measurements of etched tracks and mathematical fitting (see Li et al. 2012). Therefore, the description of the two different regimes with a single curve, especially the description of the regime with smaller S_e by a simple logarithmic equation (i.e., Eq. 2), provides an important physical form that has long been recognized as needed (Carlson 1990; Gleadow et al. 2002; Jonckheere and Chadderton 2002) for the development of physical models of FT formation and annealing. Besides the precise picture of morphologies of FTs, as demonstrated in this study, the combination of ion-irradiation with TEM and SAXS can be readily used to obtain a deeper understanding of the gradual recovery of radiation damage during annealing at the atomic-scale.

ACKNOWLEDGMENTS

The funding for this study was provided by the Office of Basic Energy Sciences of the USDOE (DE-FG02-97ER45656). Part of this research was undertaken on the SAXS/WAXS beamline at the Australian Synchrotron, Victoria, Australia. P.K. acknowledges the Australian Research Council for financial support. This paper was improved substantially by reviews and suggestions from R. Jonckheere and an anonymous reviewer.

REFERENCES CITED

- Afra, B., Lang, M., Rodriguez, M.D., Zhang, J., Giulian, R., Kirby, N., Ewing, R.C., Trautmann, C., Toulemonde, M., and Kluth, P. (2011) Annealing kinetics of latent particle tracks in Durango apatite. *Physical Review B*, 83, 064116.
- Akcoltekin, E., Peters, T., Meyer, R., Duvenbeck, A., Klusmann, M., Monnet, I., Lebius, H., and Schlegelberger, M. (2007) Creation of multiple nanodots by single ions. *Nature Nanotechnology*, 2, 290–294.
- Bursill, L.A., and Braunschauen, G. (1990) Heavy-ion irradiation tracks in zircon. *Philosophical Magazine A—Physics of Condensed Matter Structure Defects and Mechanical Properties*, 62, 395–420.
- Calderin, L., Stott, M.J., and Rubio, A. (2003) Electronic and crystallographic structure of apatites. *Physical Review B*, 67, 134106.
- Carlson, W.D. (1990) Mechanisms and kinetics of apatite fission-track annealing. *American Mineralogist*, 75, 1120–1139.
- (1993) Mechanisms and kinetics of apatite fission-track annealing—Reply. *American Mineralogist*, 78, 446–449.
- Dodd, P.E., and Massengill, L.W. (2003) Basic mechanisms and modeling of single-event upset in digital microelectronics. *IEEE Transactions on Nuclear Science*, 50, 583.
- Donelick, R.A., Ketcham, R.A., and Carlson, W.D. (1999) Variability of apatite fission-track annealing kinetics: II. Crystallographic orientation effects. *American Mineralogist*, 84, 1224–1234.
- Gleadow, A.J.W., Belton, D.X., Kohn, B.P., and Brown, R.W. (2002) Fission track dating of phosphate minerals and the thermochronology of apatite. In M.L. Kohn, J. Rakovan, and J.M. Hughes, Eds., *Phosphates—Geochemical, Geobiological, and Materials Importance*, 48, 579–630. Reviews in Mineralogy and Geochemistry, Mineralogical Society of America, Chantilly, Virginia.
- Green, P.F., and Durrani, S.A. (1977) Annealing studies of tracks in crystals. *Nuclear Track Detection*, 1, 33–39.
- Hebert, S., Hervieu, M., Hardy, V., Aouaroun, T., Simon, C., Provost, J., Milani, E., Aruta, C., and Balestrino, G. (1998) Pillar defects, a new type of track in Pb-irradiated Bi-2212 thin films: Nanostructural study and influence on the irreversibility line. *Nuclear Instruments & Methods in Physics Research Section B—Beam Interactions with Materials and Atoms*, 142, 319–328.
- Jaskierowicz, G., Dunlop, A., and Jonckheere, R. (2004) Track formation in fluorapatite irradiated with energetic cluster ions. *Nuclear Instruments & Methods in Physics Research Section B—Beam Interactions with Materials and Atoms*, 222, 213–227.
- Jonckheere, R., and VandenHaute, P. (1996) Observations on the geometry of etched fission tracks in apatite: Implications for models of track revelation. *American Mineralogist*, 81, 1476–1493.
- Jonckheere, R.C., and Chadderton, L.T. (2002) Back to Basic? On track: The Newsletter of the International Fission-Track Community, 12, 19.
- Kluth, P., Schnohr, C.S., Pakarinen, O.H., Djurabekova, F., Sprouster, D.J., Giulian, R., Ridgway, M.C., Byrne, A.P., Trautmann, C., Cookson, D.J., Nordlund, K., and Toulemonde, M. (2008) Fine structure in swift heavy ion tracks in amorphous SiO_2 . *Physical Review Letters*, 101, 175503.
- Li, W.X., Wang, L.M., Sun, K., Lang, M., Trautmann, C., and Ewing, R.C. (2010) Porous fission fragment tracks in fluorapatite. *Physical Review B*, 82, 144109.
- Li, W.X., Wang, L.M., Lang, M., Trautmann, C., and Ewing, R.C. (2011) Thermal annealing mechanisms of latent fission tracks: Apatite vs. zircon. *Earth and Planetary Science Letters*, 302, 227–235.
- Li, W.X., Lang, M., Gleadow, A.J.W., Zdorovets, M.V., and Ewing, R.C. (2012) Thermal annealing of unetched fission tracks in apatite. *Earth and Planetary Science Letters*, 321, 121–127.
- Li, W.X., Rodriguez, M.D., Kluth, P., Lang, M., Medvedev, N., Sorokin, M., Zhang, J., Afra, B., Bender, M., Severin, D., Trautmann, C., and Ewing, R.C. (2013) Effect of doping on the radiation response of conductive Nb–SrTiO₃. *Nuclear Instruments & Methods in Physics Research Section B—Beam Interactions with Materials and Atoms*, 302, 40–47.
- Mara, A., Siwy, Z., Trautmann, C., Wan, J., and Kamme, F. (2004) An asymmetric polymer nanopore for single molecule detection. *Nano Letters*, 4, 497–501.
- Meflah, A., Brisard, F., Costantini, J.M., Hage-Ali, M., Stoquert, J.P., Studer, F., and Toulemonde, M. (1993) Swift heavy ions in magnetic insulators: A damage cross section velocity effect. *Physical Review B*, 48, 920.
- Paul, T.A., and Fitzgerald, P.G. (1992) Transmission electron microscopic investigation of fission tracks in fluorapatite. *American Mineralogist*, 77, 336–344.
- Rabone, J.A.L., Carter, A., Hurford, A.J., and de Leeuw, N.H. (2008) Modelling the formation of fission tracks in apatite minerals using molecular dynamics simulations. *Physics and Chemistry of Minerals*, 35, 583–596.
- Robinson, K., Gibbs, G.V., and Ribbe, P.H. (1971) Structure of zircon-comparison with garnet. *American Mineralogist*, 56, 782–790.
- Schouwink, P., Miletich, R., Ullrich, A., Glasmacher, U.A., Trautmann, C., Neumann, R., and Kohn, B.P. (2010) Ion tracks in apatite at high pressures: the effect of crystallographic track orientation on the elastic properties of fluorapatite under hydrostatic compression. *Physics and Chemistry of Minerals*, 37, 371–387.
- Szenes, G. (1995) General features of latent track formation in magnetic insulators irradiated with swift heavy ions. *Physical Review B*, 51, 8026.
- Vetter, J., Scholz, R., and Angert, N. (1994) Investigation of latent tracks from heavy-ions in GeS crystals by high-resolution TEM. *Nuclear Instruments & Methods in Physics Research Section B—Beam Interactions with Materials and Atoms*, 91, 129–133.
- Yamada, R., Tagami, T., and Nishimura, S. (1995) Confined fission-track length measurement of zircon—assessment of factors affecting the paleo temperature estimate. *Chemical Geology*, 119, 293–306.
- Ziegler, J.F., Ziegler, M.D., and Biersack, J.P. (2010) SRIM - The stopping and range of ions in matter. *Nuclear Instruments & Methods in Physics Research Section B—Beam Interactions with Materials and Atoms*, 268, 1818–1823.

MANUSCRIPT RECEIVED JULY 15, 2013

MANUSCRIPT ACCEPTED DECEMBER 27, 2014

MANUSCRIPT HANDLED BY DANIEL HARLOW